High-frequency permeability of porous media with thin constrictions. I. Wedge-shaped porous media

Vincent Langlois

V. Langlois, "High-frequency permeability of porous media with thin constrictions. I. Wedge-shaped porous media," Phys. Fluids 34, 077119 (2022).

High-frequency permeability of porous media with thin constrictions: I. Wedge-shaped porous media

V. Langlois[1, a)]
Navier, Univ Gustave Eiffel, Ecole des Ponts, CNRS, F-77454 Marne-la-Vallée, France

(Dated: 26 August 2022)

In this series of publications, the high-frequency behavior of the dynamic permeability of porous media with thin constriction is investigated. In part I, the classical theory of Johnson *et al.* [J. Fluid Mech. 176, 379 (1987)] for soft-curved pore geometries is recalled. For wedge-shaped pore geometries, numerical computations (by finite element method) and analysis by Cortis *et al.* [Physics of Fluids 15, 1766 (2003)] are revisited and confirmed, while leading to important new conclusions. Because the electric field is singular at the tip of wedges, the original model developed by Johnson *et al.*, which links the viscous fluid flow problem to the electrical conduction problem, is inappropriate for describing the high-frequency behavior of the viscous fluid flow through wedge-shaped porous media. In particular, in the case of small wedge angles, we show that the real part of the dynamic permeability behaves in the high-frequency regime as $\Re(k(\omega)) \propto \omega^{-(3/2)}(\ln(\omega)+\text{constant})$, which differs from the predictions of the Johnson *et al.* model [$\Re(k(\omega)) \propto \omega^{-(3/2)}$]. However, our results show that the classical Johnson *et al.* high frequency limit can be a good approximation of the viscous fluid flow if the electrical conduction problem is solved over a fluid domain truncated by a boundary layer having a thickness comparable to the viscous skin depth. In Part II, we consider foam with perforated membranes involving different microstructural characteristic lengths: pore size, membrane aperture size and membrane thickness. We assess the validity domain of the Johnson *et al.* approximation and test our modified high-frequency approximation for such porous materials.

I. INTRODUCTION

The Darcy permeability k_0 of porous media is of interest in many fields: hydrology, petroleum engineering, acoustics, and environment (subsurface contamination). Numerous studies have focused on linking this macroscopic property to geometrical parameters of the porous structure. For example, the well-known Kozeny Carman formula,[3] which relates the permeability to the specific surface, is well established for particulate media. Although this formula is sometimes considered for solid foam,[17,22] an alternative approach modeling foam as a network of pores connected by flow conductances (depending on the aperture sizes of throat separating neighbor pores) can give an accurate estimate of foam permeability.[8,20,21,23] In this approach, the permeability is deduced from the equivalent conductance of the pore network calculated as for the equivalent conductance of a network of electrical conductances. In the last decades, Johnson *et al.*,[14] from their work on dynamic permeability, suggested a formula that links the Darcy permeability, also called static permeability, to the porous microstructural parameters associated with the high-frequency behavior of the viscous fluid flow. The dynamic permeability $k(\omega)$ describes the linear relationship between the macroscopic velocity $\mathbf{U}$ of an incompressible fluid flowing through a porous medium subjected to an oscillatory pressure gradient ∇P (where ω is the angular frequency). If the dependence in time is assumed to be harmonic ($e^{i\omega t}$), the Darcy equation is transformed into a complex-valued relationship:

$$\phi \mathbf{U} = -\frac{k(\omega)}{\mu}\nabla P, \tag{1}$$

where ϕ is the open porosity and μ is the dynamic viscosity of the fluid.

The dynamic permeability is linked to the dynamic tortuosity $\alpha(\omega)$, which is a measure of the increase in the dynamic effective density of the fluid:

$$\rho(\omega) = \rho_0 \alpha(\omega) = \mu\phi/(i\omega k(\omega)), \tag{2}$$

where ρ_0 is the fluid density.

In viscous fluid flow, the no-slip condition at the pore surface leads the fluid velocity to cancel, from bulk pore volume to the pore surface, over a length called viscous skin depth δ. This length depends on the angular frequency ω, $\delta = \sqrt{2\mu/\rho_0\omega}$, and corresponds to the wavelength and the depth penetration of the shear wave generated at the pore surface in the case of an oscillating solid body immersed in a viscous fluid.[18,24] This viscous skin depth defines a fluid area located in the vicinity of the pore surface, hereafter called the viscous boundary layer. As shown by Johnson *et al.*,[14] it is possible, for soft-curved pores [Fig. 1(a)], to approximate the dynamic permeability in the high-frequency limit by:

$$\lim_{\omega\to\infty} k(\omega) = \frac{\delta^2}{2i}\frac{\phi}{\alpha_\infty}(1-(1-i)\,\delta/\Lambda), \tag{3}$$

where Λ is the viscous characteristic length and is defined as a velocity-weighted pore volume (V)-to-pore surface (S) ratio:[10,14]

$$\Lambda = 2\int_{V_f} \|\mathbf{v_p}\|^2 dV_f \Big/ \int_{S_p} \|\mathbf{v_p}\|^2 dS_p; \tag{4}$$

and α_∞ is the high-frequency tortuosity:[10,14]

$$\alpha_\infty = V_f \int_{V_f} \|\mathbf{v_p}\|^2 dV_f \Big/ \left\| \int_{V_f} \mathbf{v_p} dV_f \right\|^2, \tag{5}$$

a)Electronic mail: vincent.langlois@univ-eiffel.fr.

where $\mathbf{v_p}$ is the velocity pattern of an inviscid incompressible fluid, and V_f is the fluid volume. An example of such field pattern is the scaled electric field $\mathbf{E}'$ in a conducting fluid filling the pore space of the insulating porous medium subjected to a unit macroscopic electric field $\mathbf{e_z}$, [see Eqs. (12), (19) and (20) in Sec. II].

In particular, the Johnson *et al.* high-frequency limit predicts that the real part of the dynamic permeability is given by (leading to $\Re(k) \propto \omega^{-3/2}$):

$$\lim_{\omega\to\infty} \Re\left(k\left(\omega\right)\right) = \frac{\phi}{2\Lambda\alpha_\infty}\delta^3. \tag{6}$$

From the high- and low-frequency asymptotic solutions (involving the parameters α_∞, Λ and k_0), Johnson *et al.*[14] suggested an *ad-hoc* expression for the dynamic permeability, $k\left(\omega\right)$:

$$\frac{k_0}{k\left(\omega\right)} = \left(1 + i\frac{M}{2}\frac{\omega}{\omega_c}\right)^{1/2} + i\frac{\omega}{\omega_c}, \tag{7}$$

where $\omega_c = \mu\phi/(\rho_0 k_0 \alpha_\infty)$ and $M = \frac{8k_0\alpha_\infty}{\phi\Lambda^2}$. This expression was experimentally confirmed on porous media having a smooth geometry by Charlaix *et al.*[4] and by Smeulders *et al.*[26]. Note that, Pride *et al.*[25] modified this expression to correct the predictions of the imaginary part of $k(\omega)$ in the low-frequency limit. However, by construction, the leading term in Eq. 7 is correct in the low-frequency regime, as $k(\omega)/k0 = 1 - i\beta_P(\omega/\omega_c)$ with $\beta_P = o(1)$ (see Pride *et al.*[25] for the exact definition of β_P).

Wedge-shaped pores are common in solid foam media that are typically used as sound or thermal insulators. Indeed, in these porous materials, the constrictions between the pores can be sharp as in mineral foams [as illustrated in Fig. 1(b)],[5,19] or contain open membranes as in polymer foams.[9,12,13,27]. Moreover, during the last decades, different authors have studied, from a theoretical point of view, the dynamic permeability of these porous materials.[1,7,11,16] They have shown that a sharp wedge leads to a singularity of the electric field at the end of the wedge, and even, to a zero viscous characteristic length Λ in the case of an infinitely thin wedge (similar to a membrane of zero thickness). Therefore, the fact that, on the one hand, the electric field presents singularities on the pore surface and the fluid velocity does none, and that, on the other hand, the high-frequency regime of the fluid flow can be approximated by electrical conduction is questionable.

In this paper, we are interested in the effects of the sharp shape of inter-pore constrictions on the high-frequency dynamic behavior of the permeability. In the first section, we recall the microscopic description of the fluid velocity field leading to the expected high-frequency behavior for smoothly curved pores. Then, we focus on the modeling of corrugated pore channels and revisit the numerical calculations performed by Cortis *et al.*[7] to clarify some remaining details. Our results show that the real part of the dynamic permeability behaves in the high-frequency regime as $\Re\left(k\left(\omega\right)\right) \propto \omega^{-3/2}\left(\ln\left(\omega\right) + \text{constant}\right)$, which differs from the predictions of the Johnson *et al.* model.

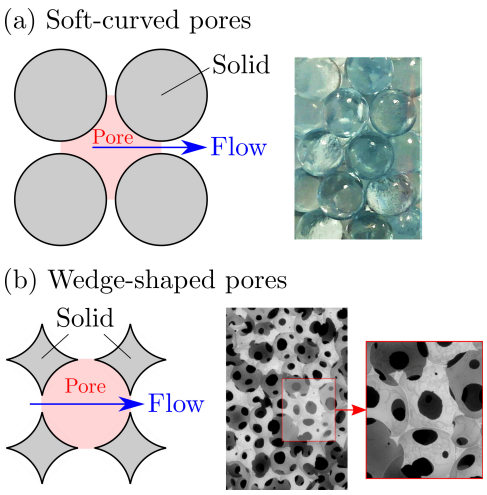

FIG. 1. Typical pore microstructures: (a) smoothly curved pores like particulate media, (b) and wedge-shaped pores like solid foam.[23]

II. THE MICROSCOPIC EQUATIONS FOR FLOW THROUGH SOFT-CURVED PORES

We consider a porous medium and denote by Ω_0 the cell that repeats periodically throughout the porous domain (with a period D_z in the direction defined by the unit vector $\mathbf{e_z}$), Ω_f the fluid domain, Ω_s the solid domain and $\partial\Omega_p$ the pore surface. With a time-harmonic macroscopic pressure gradient, the Stokes equations for the velocity field $\mathbf{v}$ of an incompressible viscous fluid saturating the porous medium are:

$$i\omega\rho_0\mathbf{v} = -\nabla p + \mu\nabla^2\mathbf{v} + \lambda_p\mathbf{e_z}, \tag{8a}$$

$$\nabla\cdot\mathbf{v} = 0, \tag{8b}$$

$$\mathbf{v} = \mathbf{0}, \text{ on the pore surface } \partial\Omega_p, \tag{8c}$$

where $\lambda_p\mathbf{e_z}$ is the macroscopic pressure gradient. Equations (8b) and (8c) correspond respectively to the mass conservation equation for incompressible fluid and the no-slip condition at the solid boundary for viscous fluid.

The pressure p represents the local pressure fluctuations around the mean value. The total fluid pressure is then equal to $p + \lambda_p z$ (within one additive constant). The macroscopic dynamic permeability can be derived from the microscopic fluid velocity (assuming isotropic behavior):

$$k\left(\omega\right) = \frac{\phi\mu}{\lambda_p}\left\langle\mathbf{v}\cdot\mathbf{e_z}\right\rangle, \tag{9}$$

where $\langle\cdot\rangle = \frac{1}{V_f}\int_{V_f}\cdot dV_f$.

The limit of the dynamic permeability $k\left(\omega\right)$ for $\omega\to 0$ is the steady-state Darcy permeability k_0, which is real-valued.

By setting $\mathbf{v}' = (i\omega\rho_0/\lambda_p)\mathbf{v}$ and $\varepsilon^2 = \mu/i\omega\rho_0 = -i\delta^2/2$, Eqs. (8) transform as follows:

$$\mathbf{0} = \varepsilon^2\nabla^2\mathbf{v}' - \mathbf{v}' - \nabla\left(p/\lambda_p\right) + \mathbf{e_z}, \tag{10a}$$

$$\nabla \cdot \mathbf{v}' = 0, \tag{10b}$$

$$\mathbf{v}' = \mathbf{0}, \text{ on the pore surface } \partial\Omega_p. \tag{10c}$$

In the high-frequency regime, $\varepsilon/D_z \to 0$, the Stokes equations [Eq. (10)] become:

$$\mathbf{0} = -\mathbf{v}'_\infty - \nabla(p/\lambda_p) + \mathbf{e_z}, \tag{11a}$$

$$\nabla \cdot \mathbf{v}'_\infty = 0, \tag{11b}$$

$$\mathbf{v}'_\infty = \mathbf{0}, \text{ on the pore surface } \partial\Omega_p. \tag{11c}$$

Therefore, in the high-frequency regime, the governing equations of the dynamic fluid flow are similar to the equations governing electrical conduction, everywhere except in the viscous boundary layer "BL" [Fig. 2(a)]:

$$\mathbf{0} = -\mathbf{E}' - \nabla V + \mathbf{e_z}, \tag{12a}$$

$$\nabla \cdot \mathbf{E}' = 0, \tag{12b}$$

$$\mathbf{E}' \cdot \mathbf{n} = 0, \text{ on the pore surface } \partial\Omega_p, \tag{12c}$$

where $\mathbf{n}$ is the unit vector normal to the pore surface, $\mathbf{E}'$ the electric field and V the perturbed electric potential. Here, $\mathbf{e_z}$ represents the forcing term, i.e. the macroscopic unit gradient of electric potential. Note that the electric field $\mathbf{E}'$ is dimensionless. Equations. (12) can also be interpreted as the equations describing the flow of an inviscid and incompressible fluid (where the scaled electrical field $\mathbf{E}'$ would correspond to the scaled velocity field of the inviscid flow $\mathbf{v}'_\mathbf{p}$). Eq. (12c) corresponds to the no-penetration condition for inviscid flow, and is less restrictive than the no-slip condition [Eq. (8c)].

Outside the viscous boundary layer, the fluid velocity can be calculated from the electric field at $O\left(\varepsilon^2\right)$ order:

$$\mathbf{v} = \frac{\lambda_p}{\mu}\varepsilon^2 \mathbf{E}'. \tag{13}$$

Cortis *et al.*[7] showed that another electric field $\varepsilon\mathbf{N}$ must be added to $\mathbf{E}'$ to have a higher order approximation of the velocity field $O\left(\varepsilon^3\right)$. This contribution is due to the normal components of the velocity created at the interface between the bulk potential flow region and the viscous boundary layer, and caused by the curvature of the pore surface. Moreover, an important property of this field is that it is orthogonal to $\mathbf{E}'$ on average : $\frac{1}{V_f}\int_{V_f} \mathbf{N}\cdot\mathbf{E}' dV_f = 0$.

Inside the boundary layer, for a frequency such that the pore surface can be considered flat (curvature radius$\gg\delta$), the fluid velocity located at the distance β from the pore surface can be approximated by:[7,18]

$$\mathbf{v}(x_p, y_p, \beta) = \frac{\lambda_p}{\mu}\varepsilon^2 \left(1 - \exp\left(-\beta/\varepsilon\right)\right)\mathbf{E}'(x_p, y_p, 0), \tag{14}$$

where x_p and y_p are the Gauss coordinates on the pore surface and, β is the distance to the pore surface (Fig. 2a). Furthermore, within the boundary layer, the electric field at the distance β from the pore surface can be approximated by the electric field at the pore surface corrected by a factor involving the ratio between β to the curvature radius of the pore surface $R(x_p, y_p)$ [see Fig. 2(b), and Appendix for full justification]:

$$\mathbf{E}'(x_p, y_p, \beta) \approx [1 - (\beta/R(x_p, y_p))]\mathbf{E}'(x_p, y_p, 0), \tag{15}$$

and consequently, in the case of soft-curved pores ($\beta < \delta \ll R$):

$$\mathbf{E}'(x_p, y_p, \beta) \approx \mathbf{E}'(x_p, y_p, 0). \tag{16}$$

For any divergence-free vector field $\mathbf{w}$ that has zero normal components on the pore surface, Cortis *et al.* showed the identity:

$$\langle \mathbf{w}\cdot\mathbf{e_z}\rangle = \left\langle \mathbf{w}\cdot\mathbf{E}'\right\rangle. \tag{17}$$

Therefore, by considering the fluid velocity $\mathbf{v}$ as the divergence-free vector field in Eq. (17) and Eqs. (13)-(16), we find:

$$\begin{aligned}\int_{V_f} \mathbf{v}\cdot\mathbf{e_z}\, dV_f &= \int_{V_f} \mathbf{v}\cdot\mathbf{E}'\, dV_f \\ &\approx \frac{\lambda_p}{\mu}\varepsilon^2\left[\int_{V_f} \|\mathbf{E}'\|^2 dV_f - \int_{\mathrm{BL}} \|\mathbf{E}'\|^2 \exp\left(-\frac{\beta}{\varepsilon}\right) dV_f\right],\end{aligned} \tag{18}$$

where, the integral over the boundary layer can be approximated by $\int_{\mathrm{BL}} \|\mathbf{E}'\|^2 \exp\left(-\frac{\beta}{\varepsilon}\right) dV_f \approx \varepsilon \int_{S_p} \|\mathbf{E}'\|^2 dS_p$.

Finally, for soft-curved pores, the dynamic permeability in the high-frequency regime can be approximated by:

$$k(\omega) = \frac{\phi\varepsilon^2}{V_f}\int_{V_f} \|\mathbf{E}'\|^2 dV_f \left[1 - \frac{\int_{S_p}\|\mathbf{E}'\|^2 dS_p}{\int_{V_f}\|\mathbf{E}'\|^2 dV_f}\varepsilon\right]. \tag{19}$$

Two important parameters, introduced by Johnson *et al.*,[14] are involved in Eq. (19):

- the tortuosity, α_∞:

$$\alpha_\infty = \frac{V_f}{\int_{V_f}\|\mathbf{E}'\|^2 dV_f} = \frac{1}{\langle\|\mathbf{E}'\|^2\rangle}, \tag{20}$$

- the viscous characteristic length, Λ:

$$\Lambda = \frac{2\int_{V_f}\|\mathbf{E}'\|^2 dV_f}{\int_{S_p}\|\mathbf{E}'\|^2 dS_p}. \tag{21}$$

By using Eq. (17) with $\mathbf{w} = \mathbf{E}'$, another expression for the tortuosity can be derived: $\alpha_\infty = 1/\langle\mathbf{e_z}\cdot\mathbf{E}'\rangle$. In this expression, $\langle\mathbf{e_z}\cdot\mathbf{E}'\rangle$ can be interpreted as the ratio of the macroscopic electrical current density J to the electrical conductivity of the fluid σ_f multiplied by the porosity ϕ. Therefore, as shown by Brown,[2] the tortuosity can be related to the effective electrical conductivity ($\sigma_e = \mathbf{J}.\mathbf{e_z} = J$) of the porous medium (assuming

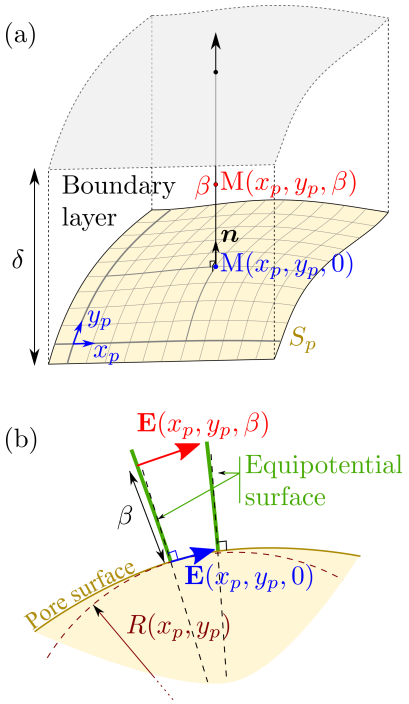

FIG. 2. (a) Local coordinates inside the viscous boundary layer. (b) Details of the electrical field in the vicinity of the pore surface.

that the solid phase is insulating): $\alpha_\infty = \phi\sigma_f/\sigma_e$. In addition, the viscous characteristic length, Λ, can be calculated from small variations in pore volume (i.e. by a uniform growth of the insulating solid phase into the pore space):[15,26]

$$\Lambda = \frac{2\int_{V_f} \|\mathbf{E}'\|^2 dV_f}{\frac{\partial}{\partial\delta_s}\int_{V_f} \|\mathbf{E}'\|^2 dV_f}, \tag{22}$$

where $(\partial/\partial\delta_s)G$ denotes the derivative of some quantity G with respect to outward virtual displacement δ_s of the pore walls.

Finally, the real and imaginary part of the dynamic permeability in high-frequency regime can be derived from Eq. (19):

$$\Re\left(k(\omega)\right) = \frac{\phi\delta^3}{4V_f} I_s, \tag{23a}$$

$$\Im\left(k(\omega)\right) = -\frac{\phi\delta^2}{2V_f}\left[I_v - \frac{\delta}{2} I_s\right], \tag{23b}$$

where $I_s = \int_{S_p} \|\mathbf{E}'\|^2 dS_p$ and $I_v = \int_{V_f} \|\mathbf{E}'\|^2 dV_f$.

III. WEDGE-SHAPED PORE CHANNEL

In this section, we consider a corrugated pore channel made from a succession of wedges (Fig. 3), and we are particularly interested in the case of very sharp edges.

A. Effect of the wedge-shape on the electric field

In the ideal case of sharp wedges, the curvature radius of the pore walls is zero at the tip of the wedge, and consequently, the electric field is singular at the tip [see from Eq. (A.2) that $\partial E(M)/\partial\beta \to \infty$ when the curvature radius tends to zero]. More precisely, the electric field is given by:[18]

$$\|\mathbf{E}'\| \propto n r^{n-1}, \tag{24}$$

where r is the distance of a point located in the pore to the tip, and $n = \pi/(2\pi - \gamma) < 1$ with γ the interior angle of the wedge (Fig. 3).

The calculation of the tortuosity α_∞ requires an integration over the pore volume which is perfectly defined even with the singularity of the electric field at the tip: $\int_{V_f} \|\mathbf{E}'\|^2 dV_f \propto \frac{n}{2} r^{2n}$. The calculation of the viscous characteristic length requires an integration over the pore surface $\int_{S_p} \|\mathbf{E}'\|^2 dS_p \propto n^2 \int_{r_0}^{r} r'^{2(n-1)} dr'$. This integral is defined if $n > 1/2$. For $n = 1/2$ ($\gamma = 0$), the wedge is infinitely sharp and the surface integral is not defined $\int_{S_p} \|\mathbf{E}'\|^2 dS_p \propto [\ln r']_{r_0\to 0}^{r} \to +\infty$. These results involving the singularity of the electric field around the tip, will make the Johnson *et al.* model inappropriate to predict the high-frequency regime of the dynamic permeability of wedge-shaped pore channels.

B. Numerical computations

We solve the boundary value problems for viscous fluid flow [Eq. (8)] and electrical conduction [Eq. (12)] by using the finite element method. Second order Lagrange elements are used for the velocity components and first order for the pressure field. The dynamic permeability $k(\omega)$ is calculated from the viscous flow solution by using Eq. (9), and the tortuosity α_∞ from the electrical conduction solution by using Eq. (20). To reduce the lack of accuracy in the numerical calculations, special care was taken to refine the mesh around the wedge tip [Fig. 3(b)]. Since the calculation of the dynamic permeability for this pore geometry has been carefully solved previously by Cortis *et al.*,[7] we have checked that our results are identical to theirs.

Figure 4 shows the real and imaginary parts of the dynamic permeability for two wedge angles ($b = \tan(\gamma/2) = 0.025$ and 0.8) as a function of ω/ω_c. It appears that the wedge angle has little effect on the dynamic permeability. Note that the characteristic frequency ω_c changes little between $b = 0.025$ and $b = 0.8$. Indeed, $k_0\alpha_\infty/(\phi L_w^2) \approx 0.098$ for $b = 0.025$, and 0.105 for $b = 0.8$.

From our numerical simulations, we revisit the analysis performed by Cortis *et al.*.[7] They proposed that the high-frequency limit derived by Johnson *et al.* be complemented by the addition of a corrective term (see below for the case of the real part $\Re(k)$, Eq. (25)). Section III C presents the numerical results and highlights how they confirm convergence toward the Cortis *et al.*[7] high-frequency limit, and not toward that of the Johnson *et al.* model. Then, we propose a new approach to approximate the high-frequency permeability.

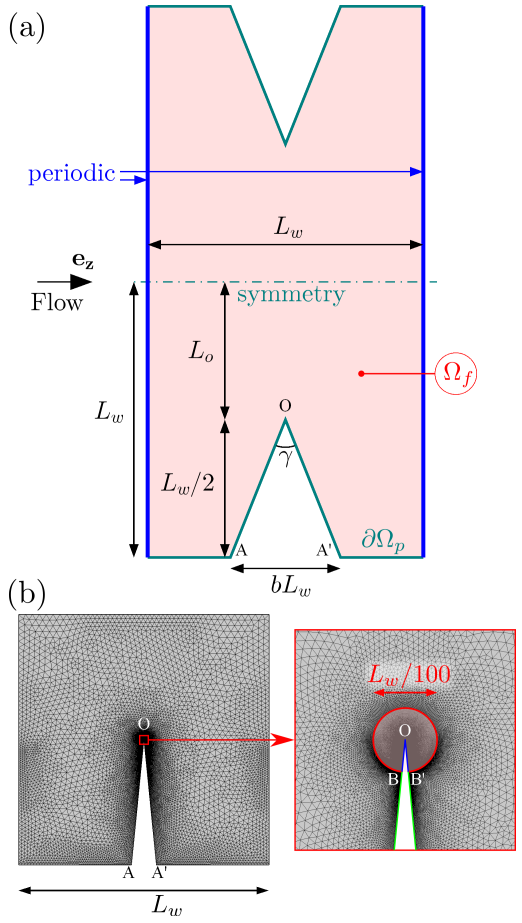

FIG. 3. Wedge-shaped pore channel. (a) Definition of the pore geometry. (b) Details concerning the mesh (the case $b = 0.1$ is used for illustration.): a maximal element size equal to $L_w/10^5$ is imposed along the line BOB' located in the vicinity of the tip ; the maximum element growth rate is equal to 1.035 in the circular area around the tip, and to 1.015 along the lines BA and B'A'.

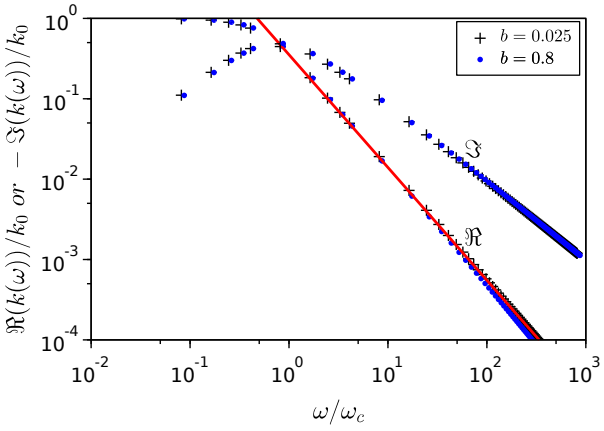

FIG. 4. Real and imaginary parts of the dynamic permeability for two wedge angles ($b = \tan(\gamma/2) = 0.025$ and 0.8) as a function of ω/ω_c. Dots correspond to FEM results, line to the predictions of Eq. (26).

C. Results and discussion

1. *High-frequency limit of the real part of* $k(\omega)$

By a detailed study of this special case, Cortis *et al.*[7] calculated the corrective term to add to the high-frequency Johnson *et al.* limit to rectify its predictions:

$$\Re\left(\frac{k(\omega)}{k_0}\right) \underset{\omega\to+\infty}{\to} \frac{\sqrt{M}}{2}\left(\frac{\omega}{\omega_c}\right)^{-\frac{3}{2}}\left[1+C_1\left(\frac{\omega}{\omega_c}\right)^{\frac{1-w}{2}}\right], \quad (25)$$

where C_1 is a numerical constant, and the exponent w is related to the wedge angle γ. Note that Eq. (25) was previously suggested by Achdou and Avellaneda.[1]

With $C_1 = 0$ and $M = \frac{8k_0\alpha_\infty}{\phi\Lambda^2}$, Eq. (25) corresponds to the expression obtained by Johnson *et al.* [Eq. (6) or Eq. (23a)]. The term $C_1(\omega/\omega_c)^{(1-w)/2}$ corresponds to the corrective term. From considerations of the magnitude order of the tip effect on the dynamic permeability, Cortis *et al.*[7] established the theoretical relationship between the exponent w and the wedge angle γ: $w = 2\pi/(2\pi-\gamma)$ (> 1). To check the validity of the proposed corrective term, Cortis *et al.*[7] determined the values of w, M and C_1 in Eq. (25) by an inverse method applied to the results of numerical simulations meticulously performed for various wedge angles. They found, from the numerical simulations, values for M and w similar to the theoretical values, and concluded that Eq. (25) is correct. To assess their findings, we have reproduced the same inverse method to our numerical FEM results and found the same agreement between the theoretical values and the values obtained by the inverse method, as shown in Fig. 5. Equation (25) combined with the values of w, M and C_1 calculated from FEM results gives very accurate predictions of the real part of $k(\omega)$ as shown in Fig. 6 (and previously by Cortis *et al.*).[7] In comparison, when the wedge angle is small, the original Johnson *et al.* model [Eq. (7)] and its high-frequency expansion [Eq. (23a)] are unable to predict the real part of $k(\omega)$ in the frequency range used in the FEM simulations.

However, as $(\omega/\omega_c)^{(1-w)/2} \to 0$ when $\omega \to +\infty$ [see Eq. (25)], one would expect the high frequency Johnson *et al.* limit to be a good approximation of the dynamic permeability once the corrective term introduced by Cortis *et al.* is negligible, i.e. $|C_1|(\omega/\omega_c)^{(1-w)/2} \ll 1$. To further investigate the convergence of $\Re(k)$ predicted by Eq. (25) to the high-frequency Johnson *et al.* limit, we need to know the values of C_1 that were not provided by Cortis *et al.*[7]. As shown in Fig. 5(a), C_1 depends on the wedge angle and is close to -1 for small wedge angles. To illustrate the extreme slowness of the convergence, consider for example that $\gamma = 0.1$ (i.e., $1-w \approx -0.016$) and $|C_1|(\omega/\omega_c)^{(1-w)/2} < 0.1$. Therefore, this condition requires $\omega/\omega_c \gtrsim 5.10^{125}$. For smaller wedge angles, the condition is more restrictive. In fact, in the expansion [Eq. (25)], the "leading" and "corrective" terms are of the same magnitude. Therefore, it is reasonable to ask whether the high-frequency behavior could be described in any other way than by seeking to correct the high frequency Johnson *et al.* limit.

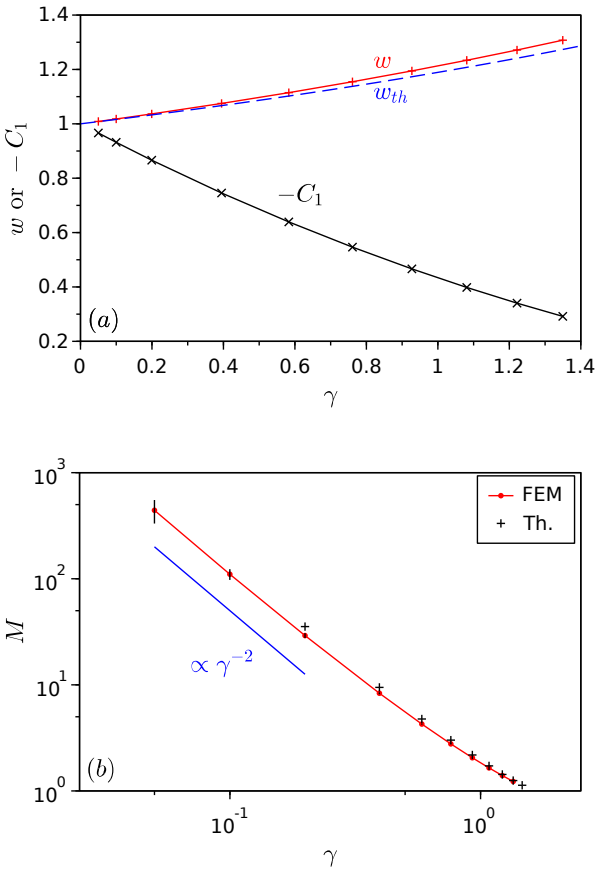

FIG. 5. Parameters w, M and C_1 [see Eq. (25)], obtained by an inverse method proposed by Cortis *et al.*[7] and applied to FEM results with various wedge angles. In (a), the values of w are compared to the theoretical values $w_{th} = 2\pi/(2\pi - \gamma)$. In (b), crosses correspond to the theoretical values calculated by Cortis *et al.*[6] with Schwartz-Christoffel transformations.

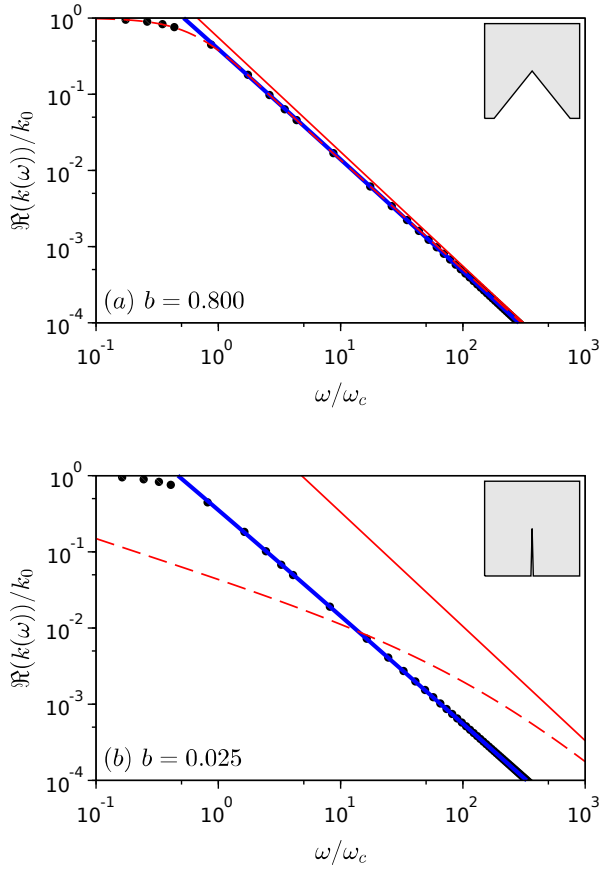

FIG. 6. Real part of the dynamic permeability for two wedge angles as a function of ω/ω_c: (a) $b = 0.8$, (b) $b = 0.025$. Dots correspond to FEM results, full red lines to the predictions of the high-frequency approximation given by Johnson *et al.* [Eq. (23a)], dashed red lines to the predictions of Johnson *et al.* model [Eq. (7)] and thick blue lines to the predictions of the Cortis *et al.* expression [Eq. (25)].

An interesting result emerges when one considers the case of small wedge angles. In that case, from numerical simulations and theoretical considerations, the parameters M, w and C_1, can be expanded as: $M \approx C_M \gamma^{-2}$ [see Fig. 5(b)], $w = 1 + C_w\gamma + o(\gamma)$ and $C_1 = -1 + C_{C_1}\gamma + o(\gamma)$ (where $C_w \approx 0.17$, $C_{C_1} \approx 0.69$ and $C_M \approx 1.15$, values determined from the results of our numerical simulations). Therefore, in the high-frequency regime, the expansion of Eq. (25) is:

$$\Re\left(\frac{k(\omega)}{k_0}\right) \underset{\omega\to+\infty}{\to} \frac{\sqrt{C_M}}{2}\left(\frac{\omega}{\omega_c}\right)^{-\frac{3}{2}}\left[C_{C_1} + \frac{C_w}{2}\ln\frac{\omega}{\omega_c}\right]. \quad (26)$$

Contrary to C_1 in Eq. (25), the coefficients C_M, C_{C_1} and C_w, are now constant and independent on the wedge angle γ (for small values of γ). As shown in Fig. 4, Eq. (26) gives very accurate predictions of the real part of the dynamic permeability in the high-frequency range (and even, for large wedge angles). Since the link with Johnson's model cancels in the calculation process leading to Eq. (26), a justification of this equation should be found elsewhere than in this model. Recall that, in Johnson's model, the real part of the dynamic permeability in the high-frequency regime is given by: $\Re(k(\omega)) = \frac{\phi\delta^3}{4V_f}\int_{S_p}\|\mathbf{E}'\|^2 dS_p$ [see Eq. (23a)]. This expression is valid for soft-curved pores for which (i) the pore surface can be assumed to be flat for the shear wave propagating in the viscous boundary layer, i.e. $\delta \ll$curvature radius; (ii) the electrical field does not change on the scale of the viscous skin depth [see Eq. (16)]. For porous media with sharp wedges, these conditions are achieved everywhere except at the wedge tip. Since the electric field is singular at the tip, the dynamic permeability predicted by the Johnson *et al.* model is influenced by the singularity of the electric field. As this singularity is specific to the electrical conduction and should not affect the dynamic fluid flow, the Johnson *et al.* model is inappropriate for predicting the high-frequency behavior of the dynamic permeability of wedge-shaped porous media. Note that, in Eq. (23a), the integration is over the pore wall surface. For soft-curved pores, since the electric field remains nearly constant at the scale of the viscous skin depth [see Eq.

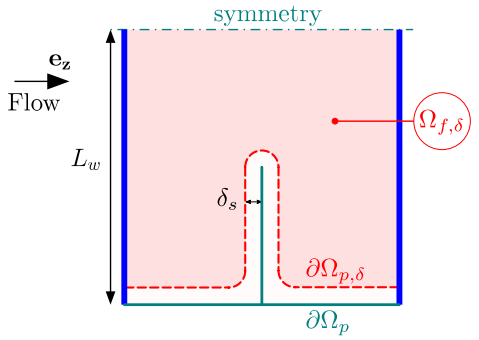

FIG. 7. Definitions of the truncated fluid domain $\Omega_{f,\delta}$ and the virtual pore surface $\partial\Omega_{p,\delta}$.

(16)], the integration could also be done (without loss of accuracy) over a virtual surface deduced by a small displacement of the pore wall toward the pore volume. Therefore, from these considerations, we propose an alternative way to approximate the high-frequency behavior of the dynamic permeability based on a pore wall shift [similar to the one used for the calculation of Λ in Eq. (22)], which allows us to define a virtual pore volume on which we solve the electrical conduction problem. The truncated fluid domain $\Omega_{f,\delta}$ is defined by excluding a boundary layer of thickness δ_s from the pore space and smoothing the virtual pore wall to obtain a minimal curvature radius equal to δ_s as illustrated in Fig. 7. The virtual shift δ_s is expected to be of the same order of magnitude as δ: $\delta_s = s\delta$ where $s = o(1)$. Finally, the real part behavior of the dynamic permeability is calculated by the following expression:

$$\Re\left(k\left(\omega\right)\right) = \frac{\phi\delta^3}{4V_f} I_{S,\delta}\left(s_s\delta\right), \tag{27}$$

where $I_{S,\delta}\left(\delta_s\right) = \int_{S_{p,\delta}} \|\mathbf{E}'\|^2 dS_{p,\delta}$ is the surface integral performed over the smooth shifted pore surface.

Note that, by using this smooth shifted pore surface, any singularity of the electric field occurring at the real pore surface is removed. Moreover, this approximation is compatible with the Johnson *et al.* model in the case of soft-curved pores since the electric field varies at the scale of the pore in this specific case, and $\partial\Omega_{p,\delta} \to \partial\Omega_p$ when $\omega \to \infty$.

Figure 8(a) shows that the relationship between the surface integral of $\|\mathbf{E}'\|^2$ over the virtual pore surface $\partial\Omega_{p,\delta}$ and the thickness δ_s is in the form: $I_{S,\delta} \approx A_s \ln\left(\delta_s\right) + B_s$ when $\delta_s/L_w < 0.01$. Combining this relationship with Eq. (27), we find a result which is very similar to Eq. (26). This result is a strong argument to validate the proposed approach. Moreover, as shown in Fig. 9(a), the predictions of Eq. (27) by using $s_s = 0.5$ are in perfect agreement with FEM results with $b = 0.0125$ (the relative gap is lower than 2% in the range $s_s = 0.5 \pm 0.05$).

2. *High-frequency limit of the imaginary part of* $k(\omega)$

With respect to the imaginary part of $k\left(\omega\right)$, Fig. 10 shows again, that the Johnson *et al.* model does not predict the high

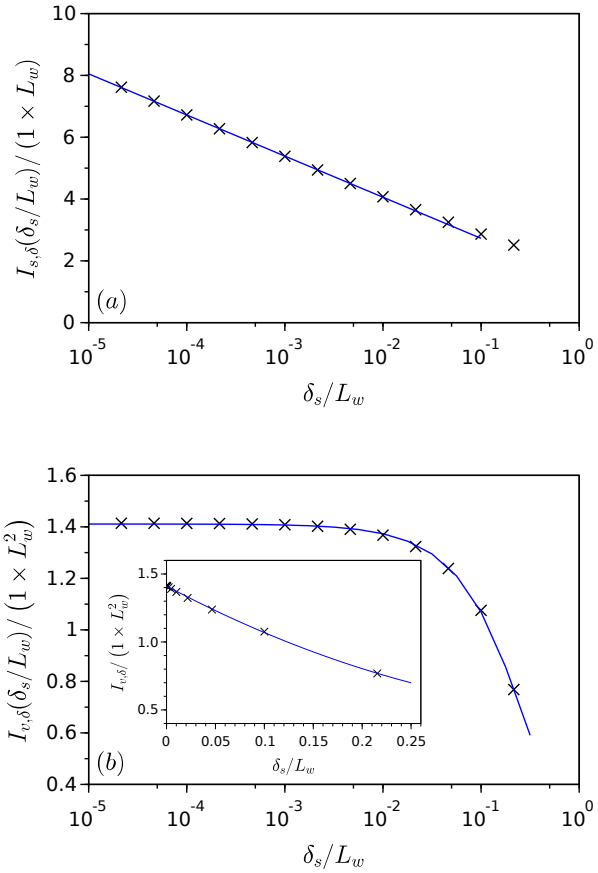

FIG. 8. (a) Surface integral $I_{S,\delta}$ of $\|\mathbf{E}'\|^2$ over the virtual pore surface $\partial\Omega_{p,\delta}$ as a function of the thickness δ_s of the truncated boundary layer. Crosses show the FEM results. Line is plotted by using $I_{S,\delta}/L_w \approx -0.578\ln\left(\delta_s/L_w\right) + 1.396$, and (b) volume integral $I_{V,\delta}$ of $\|\mathbf{E}'\|^2$ over the virtual pore volume $\Omega_{f,\delta}$ as a function of the thickness δ_s of the truncated boundary layer. Crosses show the FEM results. Line is plotted by using $I_{V,\delta}/L_w^2 \approx 3.816\left(\delta_s/L_w\right)^2 - 3.800\left(\delta_s/L_w\right) + 1.411$. The same data are used in (b) and its inset.

frequency regime when the wedge angle is small. Therefore, we are interested in how our virtual fluid domain based approach can be used to estimate the imaginary part of $k(\omega)$. From Eq. (23b) established for soft-curved pores, we could consider two possibilities:

$$\Im\left(k\left(\omega\right)\right) = -\frac{\phi\delta^2}{2V_f}\left[I_{V,\delta}\left(s_v\delta\right) - \frac{\delta}{2}I_{S,\delta}\left(s_s\delta\right)\right], \text{ or} \tag{28a}$$

$$\Im\left(k\left(\omega\right)\right) = -\frac{\phi\delta^2}{2V_f} I_{V,\delta}\left(s_v\delta\right), \tag{28b}$$

where $I_{V,\delta}\left(\delta_s\right) = \int_{V_{f,\delta}} \|\mathbf{E}'\|^2 dV_{f,\delta}$.

Equation (28b) is derived from Eq. (23b) by retaining only the leading order. Eq. (28a) is similar to Eq. (23b), except that it involves both the surface integral $I_{S,\delta}$ introduced earlier,and the volume integral $I_{V,\delta}$ calculated over the truncated

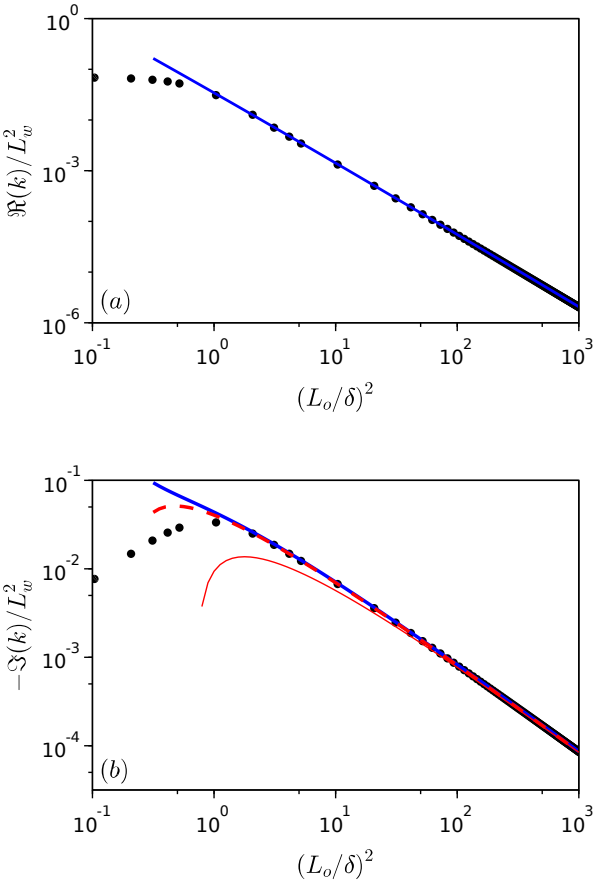

FIG. 9. (a) Real part of the dynamic permeability: FEM results with $b = 0.0125$ (dots), predictions of Eq. (27) with $s_s = 0.5$ (thick blue line). (b) Imaginary part of the dynamic permeability: FEM results with $b = 0.0125$ (dots), predictions of Eq. (28a) with $s_v = s_s = 0.5$ (red thin line) or with $s_s = 0.5$ and $s_v = 0.12$ (red dashed line), and predictions of Eq. (28b) with $s_v = s_s = 0.5$ (blue thick line). L_o is the aperture size defined in Fig.3. Note that $(L_o/\delta)^2 \propto \omega$. The transition frequency between low and high-frequency regimes corresponds to $\delta \approx L_o$.

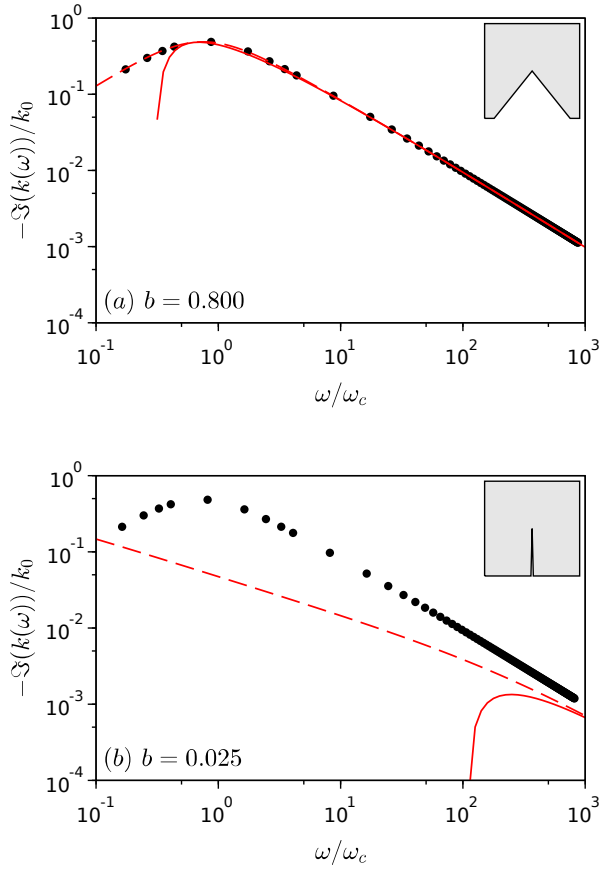

FIG. 10. Imaginary part of the dynamic permeability as a function of ω/ω_c for two wedge angles: (a) $b = 0.8$, (b) $b = 0.025$. Dots correspond to FEM results, dashed red lines to the predictions of the high-frequency approximation given by Johnson *et al.* [Eq. (23b)], and full red lines to the predictions of Johnson *et al.* model [Eq. (23)].

pore volume $\Omega_{f,\delta}$. Figure 8(b) shows that $I_{V,\delta}$ decreases as the thickness δ_s of the truncated boundary layer increases. This trend results from the progressive closure of the truncated pore volume aperture size as δ_s increases ($I_{V,\delta} = 0$ when $\delta_s = L_o$). From the inset graph of Fig. 8(b), it appears that the integral $I_{V,\delta}$ can be approximated by an expression of the form: $I_{V,\delta} \approx A_v(\delta_s)^2 + B_v(\delta_s)^2 + C_v$. Now, since the coefficient s_s is found to be equal to 0.5 (value determined from the real part of k), it remains to determine the value of the coefficient s_v in Eqs. (28). Figure 9(b) compares our FEM results obtained for a small wedge angle to the predictions of Eqs. (28) calculated with different assumptions for s_v: (i) $s_v = s_s = 0.5$ and (ii) $s_v = 0.12$ [this value is adjusted to fit the predictions of Eq. (28a) to the FEM results]. Surprisingly, it appears that Eq. (28a) requires an adjustment of the value of s_v to obtain accurate predictions of $\Im(k(\omega))$, whereas the accuracy of the predictions of $\Im(k(\omega))$ given by Eq. (28b) with $s_v = s_s = 0.5$ is remarkable over a wide range of frequencies (even when δ is close to the aperture size L_o).

3. *Application to the case of cylindrical tubes*

Since our approach seems appropriate for predicting the intermediate and high-frequency behavior of $k(\omega)$ for wedged-shaped porous media, it should also be suitable for soft-curved pores. Consider the case of fluid-saturated cylindrical tubes of radius R and length L for which the solution of $k(\omega)$ is known:[28]

$$k(\omega) = \frac{R^2}{i\kappa^2}\left(1 - \frac{2J_1(i^{3/2}\kappa)}{i^{3/2}\kappa J_0(i^{3/2}\kappa)}\right), \qquad (29)$$

where J_0 and J_1 are the Bessel functions of the zeroth and first order, respectively, and $\kappa = \sqrt{2}R/\delta$. In the high-frequency

limit, this expression can be approximated by:

$$k(\omega) = \left(\frac{\delta^3}{2R}\right)\left(1-\frac{\delta}{2R}\right) - i\left(\frac{\delta^2}{2}\right)\left(1-\frac{\delta}{R}\right) + o(\delta^4). \tag{30}$$

For this simple case, as $\|\mathbf{E}'\|^2 = 1$, $I_{S,\delta}$ and $I_{V,\delta}$ can be calculated easily: $I_{S,\delta}/V_f = (2/R)(1-(\delta_s/R))$ and $I_{V,\delta}/V_f = (1-(\delta_s/R))^2 = 1-2(\delta_s/R)+(\delta_s/R)^2$. Equations (27), (28a) and (28b) gives respectively:

$$\Re\left(k(\omega)\right) = \frac{\delta^3}{2R}\left(1-s_s\frac{\delta}{R}\right),$$

$$\Im\left(k(\omega)\right) = -\frac{\delta^2}{2}\left[1-(2s_v+1)\frac{\delta}{R}\right] + o((\delta/R)^3),$$

$$\Im\left(k(\omega)\right) = -\frac{\delta^2}{2}\left[1-2s_v\frac{\delta}{R}\right] + o((\delta/R)^3).$$

From these expressions, it is straightforward to show that Eqs. (27) and (28) are consistent with Eq. (30) when using $s_s = 1/2$ and $s_v = 0$ with Eqs. (27) and (28a), or $s_s = s_v = 1/2$ with Eqs. (27) and (28b). These values are in agreement with the results obtained for the corrugated pore channel [especially when using $s_s = s_v = 1/2$ with Eqs. (27) and (28b)].

IV. CONCLUSION

The ability of the dynamic permeability model of Johnson *et al.*[14] to predict the high-frequency behavior of wedge-shaped porous media has been investigated. The main steps leading to the high-frequency limit derived by Johnson *et al.*[14] in the case of soft-curved pores have been recalled. We have also revisited the numerical computations and the analysis by Cortis *et al.*[7] regarding the dynamic permeability of corrugated pore channels with sharp wedges. In such a pore geometry, the electric field has tip singularities, and, the use of the Johnson *et al.* model, which links the dynamic permeability to parameters defined from the electrical conduction problem, leads to a contradiction: the predicted dynamic permeability would depend on the contribution of the tip singularities of the electric field while the actual dynamic viscous flow does not. Consequently, the Johnson *et al.* model is inappropriate to predict the high-frequency limit of porous media with sharp wedges. We propose a modification of the classical Johnson *et al.* model to remove this apparent contradiction. It consists in solving the electrical conduction problem by considering a fluid domain $\Omega_{f,\delta}$ truncated by a boundary layer having a thickness δ_s comparable to the viscous skin depth, $\delta_s \approx \delta/2$. As the viscous skin depth tends to zero when $\omega \to \infty$, our approach does not alter the classical high-frequency limit of Johnson *et al.* for soft-curved pores. For such pore geometry, our approximation would lead to a frequency-dependent viscous characteristic length which tends to the classical Johnson viscous length when $\omega \to \infty$. Nevertheless, a complete theoretical justification of the proposed approximation remains to be done.

In the case of small wedge angles, we have shown that the real part of the dynamic permeability behaves in the high-frequency regime as $\Re\left(k(\omega)\right) \propto \omega^{-3/2}\left(\ln(\omega) + \text{constant}\right)$, which differs from the predictions of the Johnson *et al.* model. Experimental confirmation of this high-frequency approximation should require the use of porous media with very sharp wedges, such as monodisperse solid foams with a solid fraction between 0.12 and 0.3.[23]

In Part II of this series of publications, we will focus on testing our approach on soft-curved pores having multiple microstructure sizes l_i, such that $l_1 \ll l_2 \ll ....$

Appendix: Relationship between the electrical field and the curvature radius

In this appendix, we focus on the justification of Eq. (15). We consider a point M located on the soft-curved pore surface [Fig (11)]. We use the plane defined by the normal vector to the pore surface and the electric field at point M (which is tangent to the pore surface), and define the local Cartesian coordinates, noted y and z in this appendix. In this plane, the surface of the pore is described by a function $z_p(y)$. We assume that the pore surface is smooth, and thus, the curvature radius R_M of z_p in M is non-zero. We consider a porous material subjected to a macroscopic gradient of potential electric, and a local electrical field derived from a potential Ψ. From all these considerations, we can write in M:

$$\frac{dz_p}{dy}(\mathrm{M}) = 0,\ E_z(\mathrm{M}) = 0,\ \text{and}\ R_\mathrm{M}^{-1} = -\frac{d^2z_p}{dy^2}(\mathrm{M}). \tag{A.1}$$

Moreover, the fact that the electric field is tangent to the pore surface leads to:

$$\frac{dz_p}{dy} = -\frac{\partial\Psi}{\partial y}(y,z_p(y))\Big/\left[\frac{\partial\Psi}{\partial z}(y,z_p(y))\right],$$

and, after derivation to:

$$\begin{aligned}\frac{d^2z_p}{dy^2} =& \left[\frac{\partial\Psi}{\partial y}\left(\frac{\partial^2\Psi}{\partial y\partial z}+\frac{\partial^2\Psi}{\partial z^2}\frac{dz_p}{dy}\right)\right.\\ &\left.-\frac{\partial\Psi}{\partial z}\left(\frac{\partial^2\Psi}{\partial y^2}+\frac{\partial^2\Psi}{\partial z\partial y}\frac{dz_p}{dy}\right)\right]\left(\frac{\partial\Psi}{\partial y}\right)^{-2}\\ =& \left[E_y\left(\frac{\partial E_y}{\partial z}+\frac{\partial E_z}{\partial z}\frac{dz_p}{dy}\right)-E_z\left(\frac{\partial E_y}{\partial y}+\frac{\partial E_y}{\partial z}\frac{dz_p}{dy}\right)\right]E_y^{-2}.\end{aligned}$$

Then, by considering the point M (on the pore surface) and Eqs. A.1, we find:

$$E_y(M)R_\mathrm{M}^{-1} = -\frac{\partial E_y}{\partial z}(\mathrm{M}). \tag{A.2}$$

Finally, by using a Taylor expansion at point M for large curvature radius ($\beta/R_\mathrm{M} \ll 1$), we find Eq. (15).

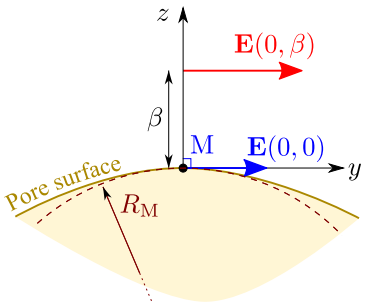

FIG. 11. Definition of the local Cartesian coordinates used for the justification of Eq. (15).

ACKNOWLEDGMENTS

The author would like to thank Cong-Truc Nguyen for his help in programming the weak formulation, Camille Perrot for his careful reading of the manuscript, and Denis Lafarge for helpful discussions and careful reading of the manuscript.

REFERENCES

[1] Achdou, Y. and Avellaneda, M., "Influence of pore roughness and pore-size dispersion in estimating the permeability of a porous medium from electrical measurements," Phys. Fluids A Fluid Dyn. **4**, 2651–2673 (1992).
[2] Brown, R. J. S., "Connection between formation factor for electrical resistivity and fluid-solid coupling factor in Biot's equations for acoustic waves in fluid-filled porous media," Geophysics **45**, 1269–1275 (1980).
[3] Carman, P. C., *Flow of Gases through Porous Media.* (Butterworths Scientific, New York, London, 1956).
[4] Charlaix, E., Kushnick, A. P., and Stokes, J. P., "Experimental Study of Dynamic Permeability in Porous Media," Phys. Rev. Lett. **61**, 1595–1598 (1988).
[5] Chevillotte, F. and Perrot, C., "Effect of the three-dimensional microstructure on the sound absorption of foams: A parametric study," J. Acoust. Soc. Am. **142**, 1130–1140 (2017).
[6] Cortis, A. and Smeulders, D. M., "On the viscous length scale of wedge-shaped porous media," Int. J. Eng. Sci. **39**, 951–962 (2001).
[7] Cortis, A., Smeulders, D. M. J., Guermond, J. L., and Lafarge, D., "Influence of pore roughness on high-frequency permeability," Phys. Fluids **15**, 1766–1775 (2003).
[8] Despois, J.-F. and Mortensen, A., "Permeability of open-pore microcellular materials," Acta Mater. **53**, 1381–1388 (2005).
[9] Doutres, O., Atalla, N., and Dong, K., "A semi-phenomenological model to predict the acoustic behavior of fully and partially reticulated polyurethane foams," J. Appl. Phys. **113**, 54901 (2013).
[10] Firdaouss, M., Guermond, J.-L., and Lafarge, D., "Some remarks on the acoustic parameters of sharp-edged porous media," Int. J. Eng. Sci. **36**, 1035–1046 (1998).
[11] Firdaouss, M., Guermond, J. L., and Le Quéré, P., "Nonlinear corrections to Darcy's law at low Reynolds numbers," J. Fluid Mech. **343**, 331–350 (1997).
[12] Gao, K., van Dommelen, J., and Geers, M., "Microstructure characterization and homogenization of acoustic polyurethane foams: Measurements and simulations," Int. J. Solids Struct. **100-101**, 536–546 (2016).
[13] Gaulon, C., Pierre, J., Derec, C., Jaouen, L., Bécot, F.-X. X., Chevillotte, F., Elias, F., Drenckhan, W., and Leroy, V., "Acoustic absorption of solid foams with thin membranes," Appl. Phys. Lett. **112**, 261904 (2018).
[14] Johnson, D. L., Koplik, J., and Dashen, R., "Theory of dynamic permeability and tortuosity in fluid saturated porous media," J. Fluid Mech. **176**, 379–402 (1987).
[15] Johnson, D. L., Koplik, J., and Schwartz, L. M., "New pore-size parameter characterizing transport in porous media," Phys. Rev. Lett. **57**, 2564–2567 (1986).
[16] Kostek, S., Schwartz, L. M., and Johnson, D. L., "Electrical Estimates," Phys. Rev. B **45**, 186–195 (1992).
[17] Lacroix, M., Nguyen, P., Schweich, D., Pham Huu, C., Savin-Poncet, S., and Edouard, D., "Pressure drop measurements and modeling on SiC foams," Chem. Eng. Sci. **62**, 3259–3267 (2007).
[18] Landau, L. D. and Lifschitz, E. M., *Fluid mechanics* (Pergamon Press, 1987) p. 539.
[19] Langlois, V., Kaddami, A., Pitois, O., and Perrot, C., "Acoustics of monodisperse open-cell foam: An experimental and numerical parametric study," J. Acoust. Soc. Am. **148**, 1767–1778 (2020).
[20] Langlois, V., Nguyen, C. T., Detrez, F., Guilleminot, J., and Perrot, C., "Permeability of polydisperse solid foams," Phys. Rev. E **105**, 015101 (2022).
[21] Langlois, V., Trinh, V. H., Lusso, C., Perrot, C., Chateau, X., Khidas, Y., and Pitois, O., "Permeability of solid foam: Effect of pore connections," Phys. Rev. E **97**, 53111 (2018).
[22] Liu, J., Wu, W., Chiu, W., and Hsieh, W., "Measurement and correlation of friction characteristic of flow through foam matrixes," Exp. Therm. Fluid Sci. **30**, 329–336 (2006).
[23] Pitois, O., Kaddami, A., and Langlois, V., "Permeability of Monodisperse Solid Foams," Transp. Porous Media **134**, 1–15 (2020).
[24] Price, P. B., "Mechanisms of attenuation of acoustic waves in antarctic ice," Nucl. Inst. Methods Phys. Res. A **325**, 346–356 (1993).
[25] Pride, S. R., Morgan, F. D., and Gangi, A. F., "Drag forces of porous-medium acoustics," Phys. Rev. B **47**, 4964–4978 (1993).
[26] Smeulders, D. M. J., Eggels, R. L. G. M., and Van Dongen, M. E. H., "Dynamic permeability: reformulation of theory and new experimental and numerical data," J. Fluid Mech. **245**, 211 (1992).
[27] Trinh, V. H., Langlois, V., Guilleminot, J., Perrot, C., Khidas, Y., and Pitois, O., "Tuning membrane content of sound absorbing cellular foams: Fabrication, experimental evidence and multiscale numerical simulations," Mater. Des. **162**, 345–361 (2019).
[28] Zwikker, C. and Kosten, C. W., *Sound Absorbing Materials* (Elsevier, New York, 1949) p. 174.